Investigating Near-Infrared Spectroscopy Imaging of Alzheimer's Through Histological Analysis

Matthew T. Kenney[1,2,] James Herpy Kinnard[1], Samantha Calderazzo[1], Dr. Douglas Rosene[1], Dr. Eugene Hanlon[3]

1. *Boston University Medical School Laboratory of Cognitive Neurobiology, Anatomy and Neurobiology (Boston University School of Medicine, Boston, Massachusetts 02118, USA)*

2. *Manchester Essex Regional High School (Manchester, Massachusetts, 01944, USA)*

3. *Department of Veterans Affairs, Office of Research and Development, and Geriatric Research, Education and Clinical Center (Bedford, Massachusetts 01730, USA)*

1. Abstract

While several existing methods can confirm the presence of Alzheimers Disease (AD) pathology in deceased patients, currently, no method has demonstrated consistent ability to definitively diagnose AD pathology in living patients. Several new techniques which show promise in *in-vivo* detection are emerging, however, which might allow for definitive Alzheimers diagnosis and monitoring of AD's pathological progression during life. In the present study, one such technique is investigated. This new technique, developed by Dr. Eugene Hanlon and associates, is referred to as near infrared spectroscopy (NIRS). The technique uses Near Infrared Light (NIR) to differentiate Alzheimer's tissue from non-AD tissue *in vitro* (Hanlon et al., 2008). According to Dr. Hanlon's unpublished data, NIRS shows a 90% success rate (personal communication, August 9, 2016) in differentiating non-AD tissue from AD tissue *in vitro*, however, it is currently unknown which features of AD tissue cause the unique optical properties of Alzheimer's tissue which are exploited by NIRS imaging. The present study attempts to discover which features allow for NIRS to effectively differentiate AD and non-AD tissue specimens. Histological analysis using immunohistochemistry and stereology, along with previously collected NIRS data provide the basis for this investigation. The present study attempts to isolate the Alzheimer's biomarkers responsible for the unique optical properties of Alzheimer's brain tissue, to attempt to validate NIRS as a reliable detector of AD, and to offer valuable data which may be further explored to discover other potential uses of NIRS. Though results are pending, this report provides data from histological analysis acquired thus far and discusses potential causes for the optical properties of AD brains. Using the data acquired through this study, NIRS imaging may potentially be improved and eventually expand its usage to the *in vivo* domain.

2. Keywords

Alzheimer's disease, diagnostic imaging, Aß plaques, PHF-tau, Near-infrared light

3. Introduction

The Need For *in vivo* Alzheimer's Imaging

Alzheimer Disease (AD) is the most common form of dementia, accounting for an estimated 60-80 percent of dementia cases seen in clinical practice (Alzheimer's Association, 2017). AD is a progressive and terminal neurodegenerative disease that is highly associated with advanced age. It presents clinically as progressively worsening memory loss often accompanied by several other symptoms including social withdrawal, a state of heightened confusion, decreased judgement capabilities, and even changes in mood or personality (Korolev, 2014). The only widely accepted forms of testing for Alzheimers which provide a definitive diagnosis, however, require neuropathologic examination, a class of techniques which are conducted almost exclusively postmortem. Neuropathologic examination techniques typically require an autopsy, and thus are unable to provide a diagnosis during a patient's life (Hanlon et. al., 2008).

A method that provides for a definitive diagnosis and the capability to monitor the progression of AD in living patients would be highly beneficial to the study of AD pathology. Furthermore, as the scientific community has continued to forge breakthrough discoveries regarding the molecular and pathological features of AD, new pharmaceutical treatment interventions are now being pursued (Hanlon et. al., 2008). It would be highly beneficial in this field of treatment discovery to be able to monitor the AD's pathological response to pharmaceutical intervention. Finally, if an *in vivo* method of detection could identify AD in preclinical stages, then treatments could be implemented to help slow or prevent the onset of symptoms before they appear.

Near-infrared Spectroscopy

In the recently published study titled *Scattering differentiates Alzheimer disease in vitro*, Dr. Eugene Hanlon and his associates explain a new imaging technique for Alzheimer's detection which may be able to be used as a diagnostic predictor of AD presence and severity in living patients (Hanlon et al., 2008). The technique they developed utilizes optical light scatter, as detected by near-infrared spectroscopy (NIRS), as a predictor of AD histopathology in the temporal lobe. The NIRS technique takes advantage of the non-

invasive, harmless nature of near-infrared (NIR) light, a frequency deemed favorable for in vivo imaging due to its relatively low tissue absorption and negligible autofluorescence (Hong G, Antaris AL, Dai H, 2017).

In this technique, the medical technology developed by Hanlon and his associates directs a beam of NIR light at the temporal lobe of the patient. The NIR light is not absorbed by the brain tissue, but rather passes directly through it. Optical sensors then measure the light diffraction that the NIR experiences as it passes through the brain. By analyzing data collected by this imaging technique, Hanlon and his partners were able to identify a clear deviation from the norm in the optical properties of Alzheimers brains– Alzheimer's brains cause an abnormally high degree of light scatter (Hanlon et al., 2008). The study thus discovered that light scatter may be leveraged to differentiate AD brains from non-demented brains. Additionally, they found that specimens labeled "severe AD" at autopsy displayed scattering values that were distinct from cases of "moderate AD" and "non-AD" pathology (Hanlon et al., 2008; Hanlon, et al. 1999). NIRS is now beginning considered as an *in-vivo* detection methodology, and shows promise in this field of work as well due to NIR light's harmless nature. NIRS, therefore, has the potential to function as a diagnostic predictor of AD pathology's presence and/or severity during preclinical and Mild Cognitive Impairment (MCI) stages, allowing clinicians to identify at-risk patients earlier in the course of AD.

By comparing postmortem autopsy reports to the results procured by NIRS, the accuracy of NIRS, in its current form, has been determined. According to Hanlon, his unpublished data shows that his method is successful in predicting Alzheimers cases with a 90% confidence interval (personal communication, August 9, 2016). Despite the apparent accuracy of the methodology, however, no study to date has correlated NIR scattering intensity with the quantified severity of AD histopathology (Hanlon et al., 2008). If the microscopic features which cause NIR scattering were discovered, researchers would likely be able to determine the range of uses of NIRS, the utility of NIRS in various subsets of the Alzheimer's population, and would be able to collect valuable calibration data to improve the accuracy of the technique.

The Present Study

Considering the numerous benefits of determining the microscopic features pertinent to NIR imaging, the present study attempts to determine the correlation between the presence AD biomarkers and NIRS light scatter data. The current study utilizes immunohistochemistry, a method to mark and identify proteins using antibodies, and stereology, a method for extracting quantitative information in tissue analysis, to attempt to isolate the biomarkers responsible for the unique optical properties of AD tissue. It utilizes a previously described application of NIRS as our source of light scatter data and uses immunohistochemistry and stereology to provide qualitative and quantitative analyses of the pathological tau and amyloid beta accumulations in the temporal lobes of confirmed AD cases. Five tissue sections were collected from the temporal lobes of three former patients whom the method of NIR imaging has been previously tested on *in-vitro*. By comparing the histological analysis collected in the current study with optical light scatter data previously collected via NIR analysis (conducted on these same tissue specimens), the AD biomarkers responsible for the light scatter may be determined.

The current study focuses on collecting histopathologic data on prevalent 3 AD biomarkers: neurofibrillary tangles (NFTs), neuropil threads (NPs), and Amyloid Beta (Aß) plaques. Currently, each of these biomarkers has been stained in each of the five tissue sections. The immunohistochemical staining results have been observed and quantified using stereology. Results for this study are pending, however, our histopathologic data results will eventually be compared against NIRS optical data. By forming correlations between p-tau density/ Aß plaque load and NIRS optical data, the present study aims to identify the biomarkers that are responsible for the unique optical properties of AD brains in order to validate and calibrate the NIRS technique for imaging. The data acquired in this study may help in allowing NIRS to expand to the *in-vivo* domain of imaging.

---

4. Materials and Methods

Tissue:

Five temporal lobes were obtained courtesy of Dr. Eugene Hanlon and the Bedford VA Medical Center at Edith Nourse Rogers Memorial Veteran's Hospital (Bedford, Ma).

Each of the temporal lobes derived from one of three Alzheimer's brains on which the NIRS Detection technique was tested during life. Informed consent was given and approved by the Bedford VA Medical Center Institutional Review Board (IRB). For all of the three subjects, a probable-AD diagnosis was issued based on longitudinal cognitive testing, and a postmortem diagnosis was confirmed for each subject by histopathologic analysis. All specimens met the Consortium to Establish a Registry for Alzheimer's Disease (CERAD) criteria for identification as "definite Alzheimer's disease" (Mirra, et.al., 1991). The current study also obtained two healthy control brains. All specimens used for this study were dissected at the posterior end of the temporal pole and included the inferior, occipital, and superior temporal sulci. Tissue blocks were several cubic centimeters in volume. These brains were fixed with formaldehyde and tissue was cut into 40 micron slices.

The temporal cortex was chosen for analysis in this study due to its vulnerability to AD pathology early in the progression of AD. Furthermore, due to its thin layer of overlaying bone and tissue, this site is optimal for *in vivo* optical analysis.

Sectioning & Processing

All tissue blocks were fixed in PLP (4% paraformaldehyde/lysine/periodate, pH 7.4) for 149-224 days at 4ºC. Cryoprotectant protocols were subsequently administered using a 24 hour incubation in 0.1M phosphate suffer (10% glycerol, 2% DMSO, pH 7.4) at 4ºC and a subsequent 14-day incubation in 0.1M phosphate buffer (20% glycerol, 2% DMS, pH 7.4) at 4ºC. All blocks were then frozen in 2-methyl-butane at -65ºC, and stored at -80ºC until sectioning. The sectioning protocol utilized a sliding microtome which moved along the coronal plane **(Figure 1).** All tissue was sectioned into 40µm slices. 16 sections of tissue, spaced 640 µm apart, composed one series, and all sections were placed into 1 of 16 vials containing a 15% glycerol in 0.1M phosphate buffer (pH 7.4) and stored at -80ºC after a 48-hour acclimation period at 4ºC. The tissue of every sixteenth slice was mounted onto a microscope slide in order to create an atlas of each temporal lobe, 1 of every 16 slices of tissue was used for IHC trial runs, and the remainder of the tissue was used for IHC.

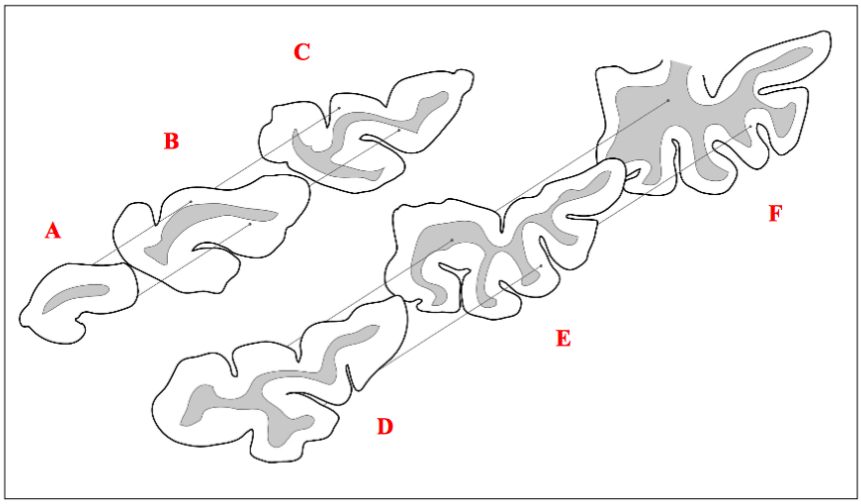

Figure 1: Representative coronal sections through the temporal pole. F is the posterior-most end of the temp. pole. Figure courtesy of James Herpy-Kinnard's work with Adobe Illustrator CS6.

Near-Infrared Spectroscopy

Note: All of the NIR work was completed prior to the current study. The excerpt below (contained within two horizontal lines) was written by James Herpy-Kinnard, another lab member who worked on this study. James received all of the following data directly from Dr. Hanlon and kindly allowed me to incorporate his work into this research report.

After being dissected, tissue blocks were flash-frozen and thawed prior to conducting NIRS. Analysis was completed at room temperature prior to staining or fixation. Each specimen was placed on a transparent coverslip and gross tissue reflectance measurements were subsequently acquired. The incident light signal was produced by a water-filtered xenon arc lamp associated with the "delivery" fiber optic at the center of six "detection" fibers. The incident signal was administered to the surface of the tissue from a distance of 10mm at an angle of approximately 30º in order to prevent confounding detection of the regular (specular) reflection of the incident light. In addition, a mirror was positioned behind the tissue to divert the path of photons that had penetrated the whole tissue. The fiber bundle terminated at a detection spectrograph (Acton SpectraPro 150) coupled to a charge coupled device (CCD) (DU-434-FI, *Andor Technology*) cooled to approximately -60ºC. Reflectance spectra for each in vitro sample were recorded from 650-1050nm.

Derivation of Scattering/ Absorption Coefficients

The absorption and scattering coefficients were based on recorded tissue relectance and transmission values using a derivation of the two-flux model, as previously described in (Hanlon et al., 2008). Observed reflectance and transmission values were analyzed using modeled parameters resulting from Monte-Carlo simulations for relevant biological tissue. The experimental scattering and absorption coefficients were determined to be the values tat gave the best-fit when applied to the modeled reflectance/ transmission spectra.

The methodology to collect *in vivo* NIRS data has not been extensively discussed as the present study intends to work with data collected *in vitro,* however, Hanlon has provided a proposed methodology to utilize NIRS *in vivo* outlined in **Figure 2**. The data eventually collected by the proposed methodology may eventually be compared against another set of histopathological data.

Figure 2: Proposed in vivo NIRS System

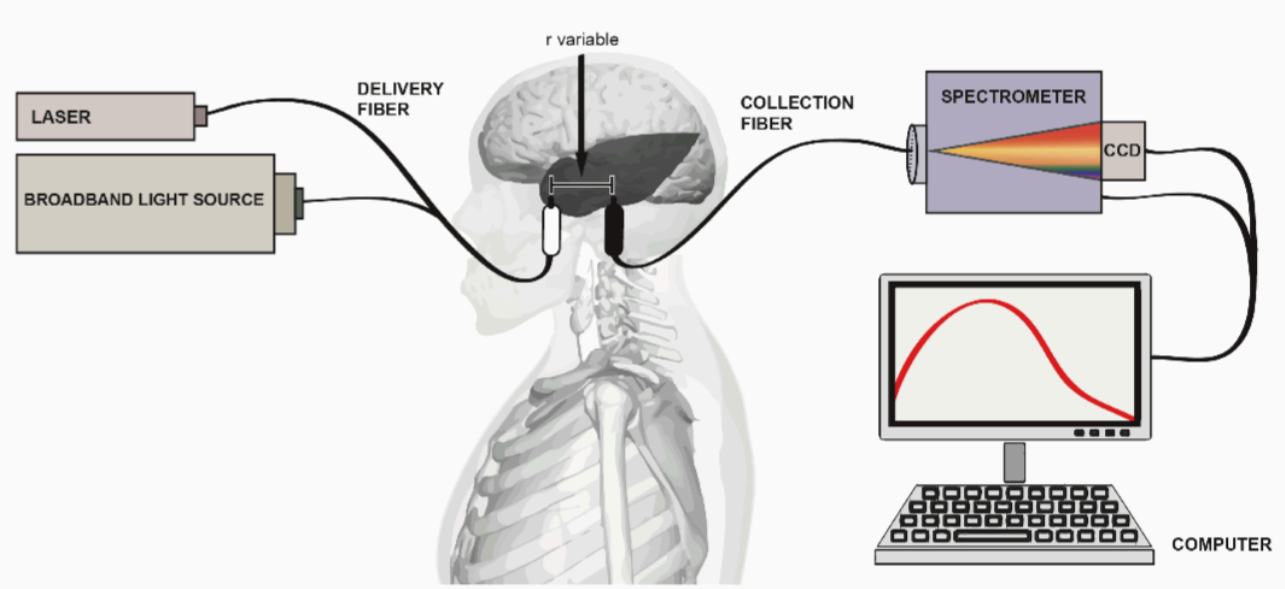

Fig. 1: In the proposed NIRS system, optical signal is delivered to the subject's head above the temporal cortex. The optical signal is detected via a collection fiber that feeds into a spectrometer. The signal is modified via charge coupled device (CCD) and the NIR spectra at a defined wavelengths interval are analyzed via computer software. Figure prepared using Adobe Illustrator CS6. Adapted from (Hanlon & Greco, 2015). Figure and caption courtesy of James Herpy-Kinnard and Dr. Eugene Hanlon.

Immunohistochemistry with APP Antibody

Our IHC protocol utilized permanent staining with chromagen, as supposed to florescence staining, because the permanent staining is far more convenient for taking stereological counts (Hoffman et. al., 2008). All sections were processed in the same reagents such that procedural variability was minimized. Our general staining procedure was as follows: One vial from each of the temporal lobe series were thawed to room temperature and processed together. Sections from each of the brain sections were thawed together and subsequently rinsed three times, for 10 min each rinse, in 2mL of 0.05M Tris buffered saline (TBS, 0.05M, pH 7.55) in order to remove all residue and cryoprotectant. Antigen retrieval was performed by incubation all section in 90% formic acid (10 minutes). After being washed again with TBS(10 min), the sections were incubated for one hour A 0.05M TBS solution containing 3% Hydrogen peroxide in order to quench endogenous peroxides. After an addition three-stage wash with TBS, using the same procedure as previously mentioned, the tissue is to be incubated for 1 hour in a blocking solution of 10% Normal Goat Serum (NGS) and 0.5% Triton X-100 in 0.05M TBS. The sections were then placed in a primary antibody solution (5% NGS, 0.5% Triton X-100 in TBS) containing the mouse monoclonal anti-amyloid precursor protein (APP) antibody 6E10 (1:1000, *Biolegend*). Sections were incubated for 24 hours at room temperature with gentle agitation in a solution containing the primary antibody buffer.

After the 24 hours, The tissue is to be washed twice more in TBS, and subsequently placed into a solution containing biotinylated goat anti-mouse secondary antibody (1:1000, *Vector Laboratories*) as well as 5% NGS and 0.5% Triton in 0.05M TBS, for one hour. Another two 10 minute washes were then conducted. The sections were then incubated with an avidin biotinylated horseradish peroxidase complex (1:200, Vectastain Standard ABC kit, Vector Laboratories) for 90 minuites. The sections are washed in the same manor again, and subsequently incubated for 8 minuites in a solution of TBS, 3′,3- diaminobenzidine (DAB, 0.05%, *Sigma*), and hydrogen peroxide (0.005%). Stained sections were mounted on gelatin-coated slides and air dried for 48 hours and were dehydrated in a series of 5 ethanol baths with concentrations of 0, 50, 70, 95, and 100%. Sections were cleared with xylene and cover slipped with Permount (*Fisher Scientific*). The same protocol was followed for negative

control tissue sections; however, the primary antibody step was excluded. No observable staining occurred in negative control samples.

PHF-tau Immunohistochemistry using the anti-PHF antibody, AT8, followed the same protocol as above, aside from two minor deviations:

1. Antigen retrieval prior to H_2O_2 incubation was performed by microwaving tissue section in 10mM sodium citrate buffer (pH 6.05) at 550 W(40ºC) for 5min., followed by 60 min incubation at room temperature in sodium citrate buffer.

2. AT8 (*Thermo Fisher*) was used at a concentration of 1:250 in primary antibody diluent (5%NGS, 0.5% Triton X-100 in TBS) and was applied at 4ºC for 48 hours.

Antibody Characterization

6E10 (*Biolegend*) is a monoclonal antibody with an epitope in amino acids 3-8 of the beta amyloid protein. The antibody is reactive to amino acid residues 1-16, and is thus bind to multiple forms of amyloid protein, including both pathological Aß and unprocessed APP (Aho, Pikkarainen, Hiltuen, Leinonen, & Alafuzoff, 2010). Only extracellular Aß plaques were used in stereologic analysis to prevent oversampling of non-pathological APP.

AT8 (Thermo Fisher) is a monoclonal antibody with an eptiope at amino acids 202 (serine) and 205 (threonine) of the tau protein. The antibody stains all 6 tau isoforms when tau is phosphorylated, as is the case with pathological PHF tau. While normally occurring tau acts as a microtubule stabilizing protein, in AD, tau proteins become phosphorylated and are mutated at a high rate, resulting in large tangles of, referred to as neurofibrillary tangles (NFTs) (Ballatore, 2007). This PHF-tau forms the characteristic neuropil threads and NFTs in the cerebral cortex of those with Alzheimer's disease (Mandelkow, et al., 1993).

Stereological Analysis

Note: Because I was not present in the laboratory for the time during which stereology was conducted, I have excerpted a description (defined between the two horizontal lines) from James Herpy-Kinnard's writing on the use of Stereology in the present study. James has also

contributed several figures to illustrate this portion of the experiment. Courtesy of James Herpy-Kinnard and Dr. Douglass Rosene.

For amyloid plaque analysis, a 10-16 section series encompassing every 16th section through the temporal pole was selected for quantification in each of the 5 cases. DAB-reactive amyloid deposits were identified using the 20x objective on Nikon E600 series microscope (Nikon, Melville, NY). The microscope was equipped with a motorized stage and encoder for z-axis measurements. The stereology software used was StereoInvestigator (MBF Biosciences) and the probe implemented was the Area Fraction Fractionator. The plaque load was estimated using the Cavalieri point counting scheme in which the reported "plaque load" represents the fraction of the temporal pole cortex occupied by DAB-reactive amyloid plaques. A positive "Plaque" marker was applied when the deployed area-fraction probe overlapped with DAB-reactive plaques, distinguishable from background staining.

The tissue areas sampled were systematically selected by the StereoInvestigator software within a user-defined region of interest (ROI) that encompassed the whole gray matter **(Figure 4)**. The ROI for each section was outlined using a 1x objective and excluded significant artefactual space or areas of damaged tissue. An area sampling fraction of 0.1127 was used to acquire an appropriate representative sample based on the the heterogeneity of plaque deposition. The parameters used with the area fraction fractionator probe are reported in **Table 1**.

The Optical Fractionator probe was used to count NFTs in a 6-9 section series encompassing every 32nd section of the temporal pole. This probe also uses systematic random sampling to yield unbiased estimates of NFT number by sampling regions within the ROI with equal probability. A pilot study was conducted to determine program specifications that meet the critical minimum values in each region of interest for the measured NFTs (grid size and dissector dimensions are reported in **Table 2**). Volume estimates of the region of interest were acquired using the reported sampling area and average tissue thickness measured at each unbiased sampling site. NFTs were identified within the dissector using a 40x objective. The counting object was immunoreactive perinuclear staining characteristic of NFTs, which was

identified by distinguishing shape, neuronal processes, and stain intensity in comparison to background (**Figure 5**). A guard limit was used to remove bias due to artefactual damage resulting from tissue sectioning above/below the dissector **(Table 2)**.

Figure 4: Cortical Region of Interest

Fig. 4: The region of interest (ROI) for stereological quantification was the cortical layers of the temporal pole. Representative slides were stained with thionin to delineate Gray/White matter boundaries. The red hashed line (top) represents the top of the established ROI. The black hashed- line (bottom) represents the bottom of the ROI. Image captured using MBF Biosciences Stereo investigator (10x magnification).

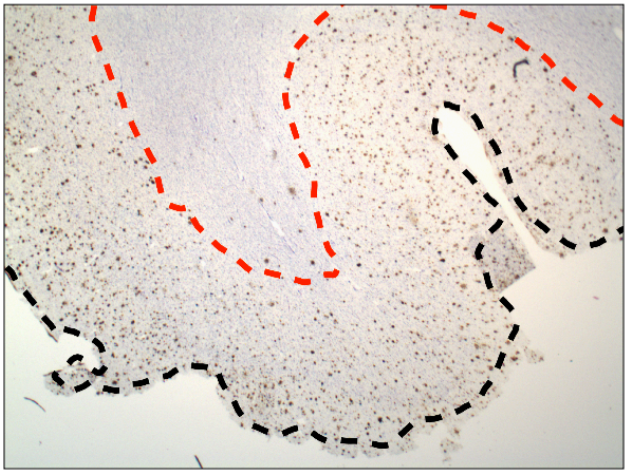

Figure 5: Optical Dissector for NFT Quantification

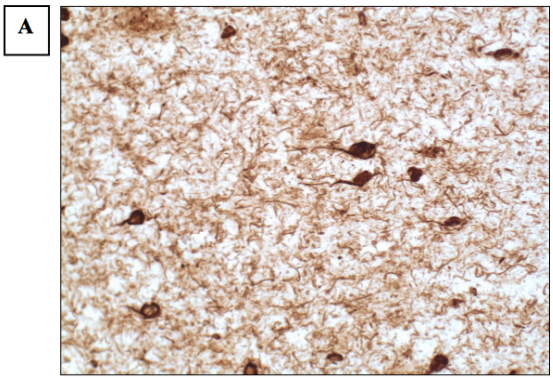

A) Systemic random sampling field chosen by StereoInvestigator software

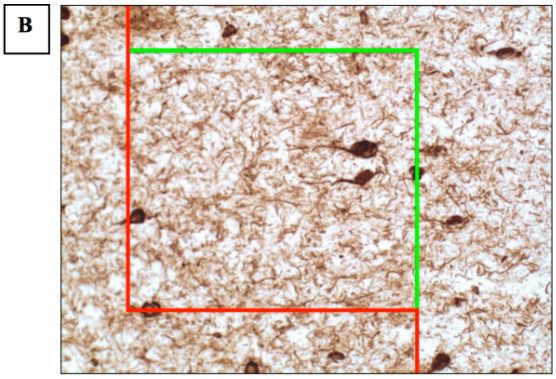

B) Schematic showing specific location of Optical Fractionator probe. Green lines indicate inclusion of countable objects. Red lines indicate exclusion of countable objects. In the above figure, 3 countable NFT are represented. Figure prepared using MBF Biosciences Stereo Investigator and Apple

Table 1: Stereological parameters for area fraction fractionator

ROI	Section Interval	Sampling Grid Area (µm²)	Counting frame area (µm²)	Dissector height (µm)	Guard Zone (µm)
Temporal Cortex	1/32	4662760	74529	20	1

Table 2: Stereological parameters for optical fractionator

ROI	Section Interval	Counting Frame (µm)	Sampling Grid (µm)	Area sampling fraction (µm)	Grid Spacing (µm)	Avg. Sites Sampled
Temporal Cortex	1/16	650 x 650	2500 x 1500	0.1127	65	963

5. Results

Overview

At the current point in the study, the first two steps of our experimentation—immunohistochemistry and stereology— have been completed. Data has not yet been acquired from Dr. Hanlon's NIRS optical data; therefore, no correlations have yet been drawn between any biomarker(s) and the heightened optical scatter seen in NIRS analysis of AD tissue.

Immunohistochemical and Stereological Results

All 5 temporal lobes thus far have demonstrated immunoreactivity to both AT8 and 6E10 antibodies. AT8 has uncovered the presence of PHF- tau in all of the culminating in both NFTs and neuropil threads as shown in two of the specimens in **Figure 6**.

The antibody utilized to stain for Aß plaques and APP, antibody 6E10, also demonstrated immunoreactivity in all 5 tissue sections, as shown below in **Figure 7.**

Figure 6: Immunoreactivity of AT8 of VA003 and VA004

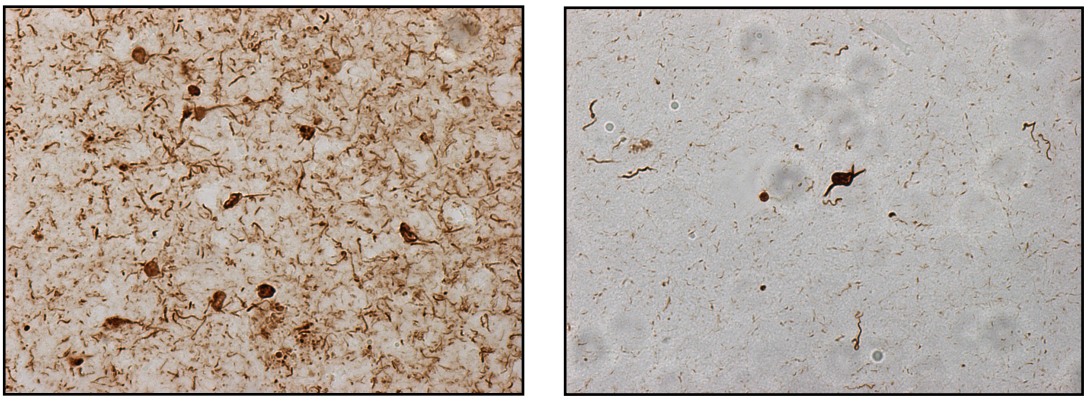

Figure 6: Stained tissue sections shown from 2 of the 5 AD temporal lobes used in our study, VA003 (left) and VA004 (right). Immunostaining was performed with tau antibody AT8, and diaminobenzidine (DAB) was used as the substrate. The large collections of p-tau resembling cell-bodies are Neurofibrillary tangles (NFTs) whereas the smaller, string-like strains of tau are known as (NPs). Both slides depict immunostaining with AT8 at 1:200 dilution and 200x magnification. Images courtesy of Dr. Douglas Rosene, Dept. of Anatomy & Neurobiology at

---

Figure 7: Amyloid Plaque IHC

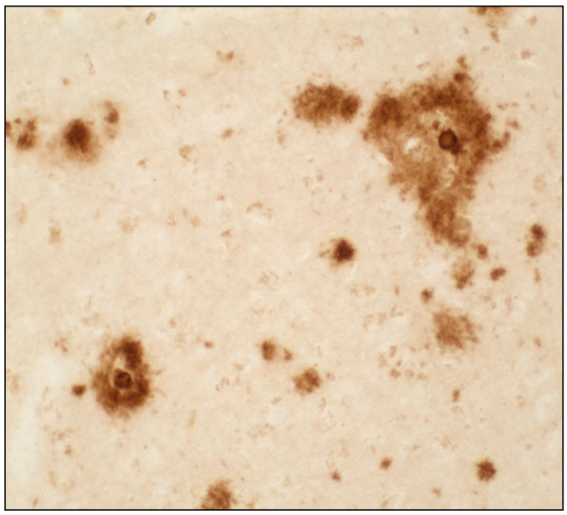

Figure 7: Displayed are two 6E10-positive dense core plaques located in the temporal pole cortex. Dense core plaques are a hallmark histopathological feature of AD, and are typically surrounded by dystrophic neurites and activated microglia (not shown). Image captured using Stereo Investigator (MBF Biosciences) at 200x magnification. Image and caption courtesy of Jimmy Herpy-Kinnard and Dr. Douglas Rosene.

None of the negative control samples exhibited observable staining for AT8 or 6E10, indicating that staining on the 5 AD samples was accurate.

Stereology

In the present study, the antibody CP13 was also utilized in IHC due to its ability to stain for forms of PHF-tau which appear in the early stages of AD. To date, however, no stereological data has yet been collected on CP13 staining.

Tissue stained with either AT8 or 6E10, however, was put through extensive stereological testing. As described in the methods section of this paper, an area fraction fractionator probe was utilized to analyze the presence of Aß by counting Aß plaque load. Alternatively, an optical fractionator was used to investigate PHF-tau by determining NFT density throughout each temporal lobe. Each of the temporal lobes varied in terms of both plaque load and NFT density, with some samples exhibiting a relatively higher plaque load than other samples but still maintaining a lower NFT density. The results of our stereological measurements are outlined below in **Table 3**.

Table 3: Alzheimer's Disease Pathology Quantification

Sample	NFT Density (tangles/mm^3)	Sections counted
VA1	2359.2	6
VA2	2155.6	7
VA3	3430.0	9
VA4	994.3	6
VA5	633.2	6

Sample	Plaque Load	Sections counted
VA1	0.1279	12
VA2	0.1228	16
VA3	0.16048	13
VA4	0.08637	10
VA5	0.09420	12

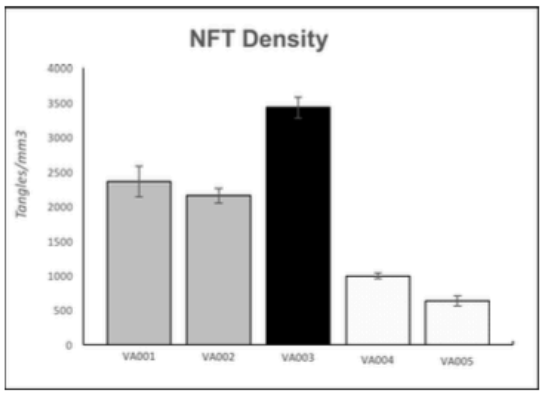

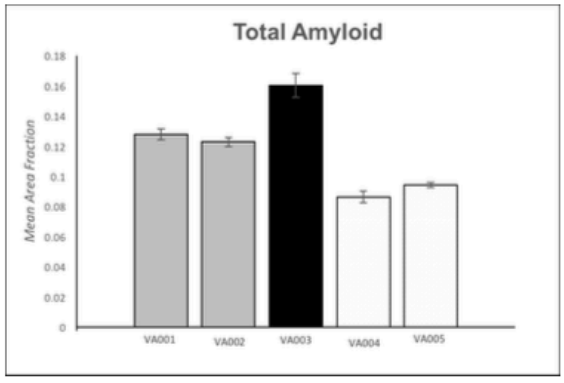

Table 3: NFT density of each sample was gathered by using an optical fractionator probe to investigate PHF-tau by determining NFT density throughout each temporal lobe. Amyloid Plaque Load was determined by using an area fraction fractionator probe. Table and Figures courtesy of Dr. Douglas Rosene

6. Discussion

The accuracy of the NIR imaging technique may be greatly improved if the present study could correlate light scatter with one or multiple microscopic features. If the present study proves successful in forming such a correlation, NIRS imaging and subsequent data analysis could potentially be further calibrated by fine tuned to ignore confounding variables. Furthermore, by providing a correlation the scope of NIRS's capabilities may be determined.

Although, presently, the experimentation in this study has not progressed to a stage where it is possible to determine which of the distinguishing biomarkers in AD contribute to heightened light diffraction, sufficient data is present to discuss the implications each biomarker might have.

Although, presently, the experimentation in this study has not progressed to a stage where it is possible to determine which of the distinguishing biomarkers in AD contribute to heightened light diffraction, sufficient data is present to discuss the implications each biomarker might have.

The Tau Protein

Based upon current findings, it is highly likely that p-tau plays a role in the heightened light diffraction seen in NIR imaging of AD tissue. Relative to other biomarkers of AD, NFTs are large and highly prevalent in AD brains and thus are likely to be a contributing factor to the increased NIR diffraction observed in NIR imaging. If further investigation in the present study demonstrates that p-tau is, in fact, a primary cause of light diffraction, this may have implications on the future of NIR imaging. If a high correlation can be determined between NFTs and the amount of diffraction recorded during NIR Imaging,

then it may be possible to expand the scope of the NIR imaging. It has been shown that the number of neurofibrillary tangles correlate with cognitive decline, and that NFT count is a significantly more reliable predictor of cognitive decline than the quantity of Aß plaques (Nelson PT, Alafuzoff I, Bigio EH, et al., 2012). Thus far, the imaging is only intended to determine whether or not Alzheimers is present, however, if a strong correlation between diffraction and tau was determined, then NIRS may be able to make predictions about how far the AD has progressed. Higher diffraction would indicate a higher number of NFTs, which in turn would indicate a greater degree of cognitive decline. In addition to this capability, if pre-symptomatic forms of tau also show a capacity to cause light diffraction, then the NIR imaging may be able to detect AD in the pre symptomatic stages. The present study may be able to determine correlations between preclinical PHF-tau forms and NIRS data by conducting stereology with CP13 immunoreactive samples.

Complications with the outlined expansions to the scope of the NIR imaging may arise, however, if tau is not the sole factor causing the heightened light diffraction. If, for instance, Aß is also shown to have a correlation with heightened diffraction readings, then the process of determining the stage of Alzheimers may be complicated. Aß has been shown to vary from case-to-case in Alzheimers and does not correlate as well with cognitive impairment (Nelson PT, Alafuzoff I, Bigio EH, et al., 2012); therefore, if Aß is also correlated with light diffraction, NIR imaging might only act as a general guideline to the progression of AD and may fail to offer accurate predictions of cognitive decline.

Amyloid Beta

Based upon the size of Amyloid beta deposits and their prevalence in AD, this characteristic biomarker of AD is also likely contribute, to some extent, to heightened light

diffraction in NIR imaging. In the case that Aß alone is responsible for the heightened light diffraction caused by AD tissue, the scope of NIRS may have a much smaller range of applications. If Aß is the sole or primary cause of light scatter, then it is unlikely that NIRS would be able to diagnose preclinical AD because significant Aß plaque load does not culminate in Aß pathology until after preclinical stages of AD (Nelson PT, Alafuzoff I, Bigio EH, et al., 2012). Furthermore, though NIRS would most likely still prove effective at determining the presence of AD in MCI or severe stages of AD, it may not be able to accurately predict cognitive decline, as previously explained.

Future Study:

If the present study does not yield any correlations, then future studies may need to be conducted to determine the cause of heightened NIR light scatter in AD temporal lobes. Furthermore, after the completion of this study, future studies may involve determining if NIR imaging is also sensitive to other tauopathies or neurodegenerative diseases. If other tauopathies or neurodegenerative diseases are identified in the same manor as AD pathology, potential complications may arise as NIRS may not be able to differentiate between these diseases. Other studies may involve further investigation into the relationship between light scatter readings collected by NIRS from AD samples and cognitive decline.

7. Bibliography

1. Aho L1, Pikkarainen M, Hiltunen M, Leinonen V, Alafuzoff I. Immunohistochemical visualization of amyloid-beta protein precursor and amyloid-beta in extra- and intracellular compartments in the human brain. Journal of Alzheimer's Disease, vol. 20, no. 4, pp. 1015-1028, 2010

2. Alzheimers Association. *Alzheimer's Disease Facts and Figures. Alzheimer's Assocation*. Alzheimers Dement 2017;13:325-373.

3. Ballatore C, Lee VM, Trojanowski JQ. Tau-mediated neurodegeneration in Alzheimer's disease and related disorders. *Nat Rev Neurosci* 2007, 8(9), pp.663-672.

4. De Matos LL, Trufelli DC, de Matos MGL, da Silva Pinhal MA. Immunohistochemistry as an Important Tool in Biomarkers Detection and Clinical Practice. *Biomarker Insights*. 2010;5:9-20.

5. Hanlon EB, Itzkan I, Dasari RR, Feld MS, Ferrante RJ, McKee AC, Lathi D, Kowall NW. Near-infrared fluorescence spectroscopy detects Alzheimer's disease in vitro. *Photochemistry and Photobiology.* 1999; 70: 236–242.

6. Hanlon EB, Perelman LT, Vitkin EI, Greco FA, McKee AC, Kowall NW. Scattering differentiates Alzheimer disease in vitro. *Opt Lett.* 2008;33(6):624–626.

7. Hoffman GE, Le WW, Sita LV. The importance of titrating antibodies for immunocytochemical methods. *Curr Protocols in Neuroscience*. 2008; Chapter 2 (Unit 2.12)

8. Hong G, Antaris AL, Dai H. Near-infrared fluorophores for biomedical imaging *Nature Biomedical Engineering* 2017;10.1038/s41551-016-0010

9. Mirra SS, Heyman A, McKeel D, Sumi SM, Crain BJ, Brownlee LM, Vogel FS, Hughes JP, van Belle G, Berg L. The Consortium to Establish a Registry for Alzheimer's Disease (CERAD). Part II. Standardization of the neuropathologic assessment of Alzheimer's disease. *American Academy of Neurology* 1991. vol. 41 no. 4 479.

10. Nelson PT, Alafuzoff I, Bigio EH, et al. Correlation of Alzheimer Disease Neuropathologic Changes With Cognitive Status: A Review of the Literature. *Journal of neuropathology and experimental neurology.* 2012; 71(5):362-381.

11. Schmitz C, Hof PR. Design-based stereology in neuroscience. 2005; *Neuroscience* 130: 813–831.